PROCEEDINGS OF SPIE

SPIEDigitalLibrary.org/conference-proceedings-of-spie

Hybrid system for in vivo real-time planar fluorescence and volumetric optoacoustic imaging

Zhenyue Chen, Xosé Luís Deán-Ben, Sven Gottschalk, Daniel Razansky

Zhenyue Chen, Xosé Luís Deán-Ben, Sven Gottschalk, Daniel Razansky, "Hybrid system for in vivo real-time planar fluorescence and volumetric optoacoustic imaging," Proc. SPIE 10494, Photons Plus Ultrasound: Imaging and Sensing 2018, 104946C (19 February 2018); doi: 10.1117/12.2287341



Event: SPIE BiOS, 2018, San Francisco, California, United States

Hybrid system for in vivo real-time planar fluorescence and volumetric optoacoustic imaging

Zhenyue Chen^a, Xosé Luís Deán-Ben^a, Sven Gottschalk^a, and Daniel Razansky^{a,b,*}
^a Institute for Biological and Medical Imaging (IBMI), Helmholtz Center Munich, Ingolstaedter

Landstr. 1, 85764 Neuherberg, Germany.

^b Faculty of Medicine, Technical University of Munich, Ismaninger Str. 22, 81675 Munich,

Germany.

ABSTRACT

Fluorescence imaging is widely employed in all fields of cell and molecular biology due to its high sensitivity, high contrast and ease of implementation. However, the low spatial resolution and lack of depth information, especially in strongly-scattering samples, restrict its applicability for deep-tissue imaging applications. On the other hand, optoacoustic imaging is known to deliver a unique set of capabilities such as high spatial and temporal resolution in three dimensions, deep penetration and spectrally-enriched imaging contrast. Since fluorescent substances can generate contrast in both modalities, simultaneous fluorescence and optoacoustic readings can provide new capabilities for functional and molecular imaging of living organisms. Optoacoustic images can further serve as valuable anatomical references based on endogenous hemoglobin contrast. Herein, we propose a hybrid system for *in vivo* real-time planar fluorescence and volumetric optoacoustic tomography, both operating in reflection mode, which synergistically combines the advantages of stand-alone systems. Validation of the spatial resolution and sensitivity of the system were first carried out in tissue mimicking phantoms while in vivo imaging was further demonstrated by tracking perfusion of an optical contrast agent in a mouse brain in the hybrid imaging modalities, making it especially useful for accurate monitoring of fluorescence-based signal dynamics in highly scattering samples.

Keywords: Optoacoustic, photoacoustic, fluorescence, imaging, tomography, 3D, hybrid system, multimodality

1. Introduction

Fluorescence imaging is widely employed in life sciences due to its powerful contrast and high molecular sensitivity. However, the low spatial resolution and lack of depth information, especially in strongly scattering samples, restrict its applicability for deep tissue imaging applications. Optoacoustic (OA) imaging possesses a highly complementary and unique set of capabilities for biological discovery, such as high spatial resolution in noninvasive deep tissue observations, fast volumetric imaging capacity and spectrally enriched contrast [1,2]. To this end, a number of approaches have been suggested for combining fluorescence and OA measurements. The performance of OA tomography (OAT) and fluorescence molecular tomography (FMT) has been compared using two stand-alone systems with ICG as a contrast agent [3]. It has been further demonstrated that the image quality of FMT reconstructions can be improved using a priori information of the optical absorption distribution rendered with OAT [4]. Two separate OA and planar fluorescence systems were employed to map sentinel lymph nodes and lymphatic vessels in rats [5]. Kosik et al. built a combined OA and trans-illumination fluorescence imaging system and demonstrated imaging of ICG flow in a phantom [6]. Hybrid microscopes for superficial imaging applications have further been constructed [7, 8]. However, all the aforementioned solutions were not suitable for simultaneous deep-tissue imaging in both fluorescence and OA modes while the relatively slow acquisition further hindered the efficient acquisition of dynamic in vivo phenomena, such as organ motion or rapid perfusion. Efficient hybridization is also hampered by the limited accessibility of the imaged area when attempting to collect high-quality data in both fluorescence and OA modes, the latter also necessitating liquid acoustic coupling and large tomographic coverage for optimal three-dimensional (3D) image quality [9].

*Corresponding author: dr@tum.de

Photons Plus Ultrasound: Imaging and Sensing 2018, edited by Alexander A. Oraevsky, Lihong V. Wang, Proc. of SPIE Vol. 10494, 104946C ⋅ © 2018 SPIE ⋅ CCC code: 1605-7422/18/\$18 ⋅ doi: 10.1117/12.2287341

2. Methods

2.1 System setup

To achieve simultaneous epifluorescence and OA volumetric imaging, a hybrid system was built based on the integration of a specifically-designed electron multiplying charge-coupled device (EMCCD)-based fluorescence fiberscope into a spherical ultrasound transducer array optimized for four dimensional (4D or real-time 3D) OA imaging performance (Fig. 1) [10]. The scope shaft (Zibra Corporation, USA) integrates a 1.4 mm fiber optic image guide composed of 100,000 fibers (Inset A in Fig. 1) along with an illumination bundle comprised of 7 silica fibers with 600 μm diameter and 0.4 numerical aperture (Insets B, C in Fig. 1). The EMCCD camera (Andor Luca R, Oxford Instruments) has an active image area of ~ 8x8 mm, corresponding to 1004x1002 pixels with size 8x8 μm. It has a high spectral sensitivity at visible and NIR wavelengths with extremely low noise. The transducer array features a central 8 mm cylindrical opening that matches the outer diameter of the shaft of the scope (Inset D in Fig. 1) and it consists of 512 piezocomposite elements disposed on a spherical surface with 40 mm radius covering an angle of 140°. Both fluorescence and OA responses are excited with the same nanosecond-duration laser pulse guided via the illumination fiber bundle integrated into the fiberscope.

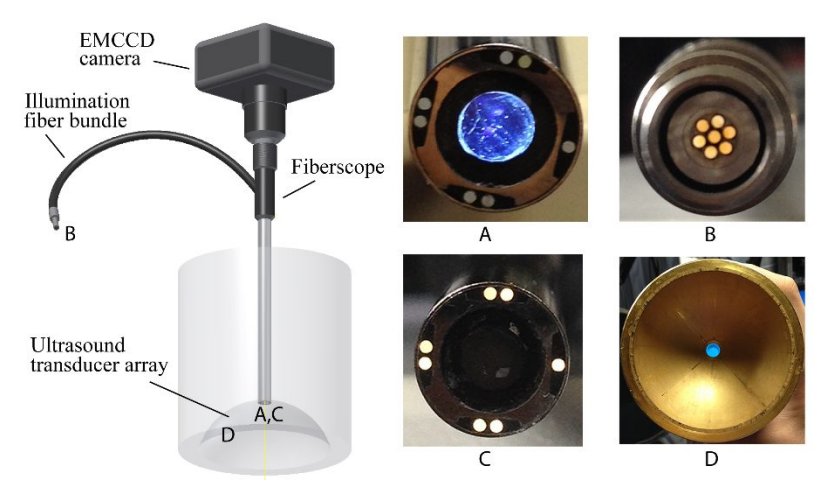


Figure 1. Layout of the hybrid planar fluorescence system. Photographs of the imaging bundle, input and output ends of the illumination bundle as well as the transducer array are shown in insets A, B, C and D.

2.2 Spatial resolution test and sensitivity comparison

System characterization was performed using USAF 1951 resolution target and controlled experiments in tissue mimicking phantoms containing deeply embedded fluorescence contrast agents. For the spatial resolution test, white light was coupled into the illumination bundle of the fiberscope. Band-pass optical filters with 525 nm (±19.5 nm, Thorlabs MF525-39) and 800 nm (±20 nm, Andover 800FS40-25) were successively placed in front of the camera and the corresponding images were acquired. A third acquisition with no filter was further performed. The same USAF target was used to evaluate the OA resolution in the lateral x-y plane. The sensitivity was tested by imaging a 0.58 mm inner diameter and 0.96 mm outer diameter polyethylene tube (Smiths Medical ASD Inc., USA) filled with different concentrations of Alexa Fluor 700 (AF700, Invitrogen, Eugene, OR, USA) [11], Alexa Fluor 750 (AF750, Invitrogen, Eugene, OR, USA) [11], indocyanine green (ICG, PULSION, Germany) [12] and IRDye 800CW Maleimide (LI-COR, USA) [13] (Fig. 2). The tubing was immersed in a phantom tank containing 33.3% (v/v) of 3.5%-fat milk and 0.1 % (v/v) of diluted India ink with 125 OD (Higgins Waterproof Black India Ink, USA), aimed at mimicking average tissue optical absorption and scattering coefficients ^[14]. The laser wavelength was tuned to 770 nm to excite ICG and IRDye 800CW, and to 680 nm and 749 nm to excite AF700 and AF750, respectively. Imaging was performed by setting the pulse repetition frequency (PRF) of the laser to 10 Hz. The excitation light fluence at the surface of the tissue-mimicking medium was ~5 mJ/cm². For AF700, a long pass filter (Edmund Optics, Stock # 62-980, USA) with 700 nm cut-on wavelength was placed in front of the camera. On the other hand, a long pass filter (Edmund Optics, Stock # 66-227, USA) with 800 nm cut-on wavelength was employed for ICG, AF750 and IRDve 800CW. The integration time of the EMCCD camera was set to 0.1 s. Both fluorescence and OA signals were averaged over 1 s, corresponding to 10 fluorescence and OA frames. Detection sensitivity performance of both imaging modalities as a function of target depth

was compared in phantoms while *in vivo* imaging performance in the hybrid mode was further corroborated by non-invasive visualization of fast contrast agent perfusion in mice.

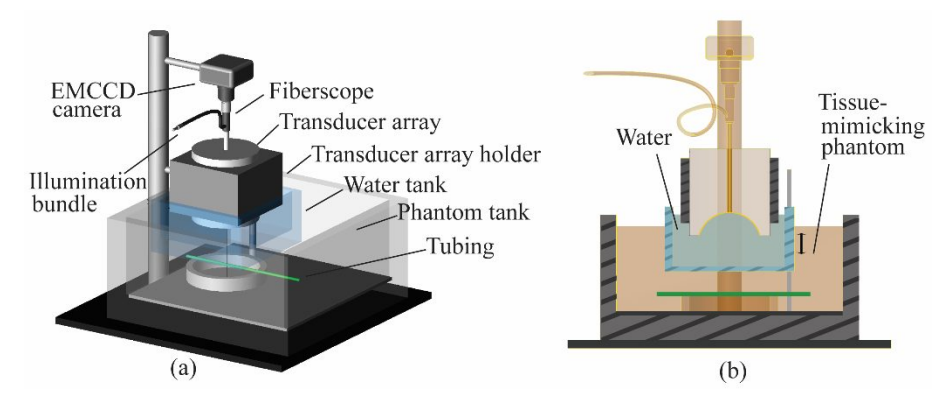


Figure 2. Lay-out of the experimental set-up for sensitivity comparison. (a) Three-dimensional lay-out of the set-up; (b) Cross sectional view of (a). Phantom tank was filled with a tissue mimicking medium. Water tank was filled with purified water to couple the acoustic signal from the tubing to the transducer array. During the experiment, only the water tank was translated up and down to change the depth of the tubing within the tissue-mimicking medium.

2.3 In vivo imaging experiment

The synergetic advantages of the hybrid system in real-time in vivo experiments were analyzed by imaging two 64 days old athymic nude-Fox1nu mice (Harlan Laboratories LTD, Switzerland). In particular, the brain region was imaged following a tail vein injection of ICG. The ICG concentration after dilution was 750 μ g/ml (~1 mM), and the injected volume was 100 μ l. The mice were first anesthetized with 1-2% Isoflurane in Oxygen at 0.7-0.8 l/min. Imaging was performed transcranially but the scalp was partially removed to evaluate how it affects imaging performance in both modalities. The laser was set to a wavelength of 700 nm and a pulse repetition rate of 25 Hz. The camera integration time was set to 0.1 s. A long pass filter (Edmund Optics, Stock # 66-227) with 800 nm cut-on wavelength was placed in front of the camera. Time-lapse fluorescence and OA data were acquired for a total duration of 300 s, starting ~10 s prior to the ICG injection. Animal handling and surgical procedures were performed according to the directives on animal experimentation of the Helmholtz Zentrum München and with approval from the Government District of Upper Bavaria.

3. Results and discussion

Fig. 3 shows the spatial resolution characterization of the hybrid system. The fiberscope achieved optical imaging of superficial targets over a large spectral range in the visible and near-infrared waveband. Images of the entire USAF target acquired through the 525 nm band-pass filter and its zoom in are shown in Figs. 2(a) and 2(b), respectively. The corresponding images for the 800 nm wavelength and white light illumination are further displayed in Figs. 2(c) and 2(d). The indicated line profiles allow identifying the thinner lines that can be resolved, which provides an estimate of the image resolution. The resolution achieved when no filter was used (white light) was approximately 20.16 lp/mm (group 4, element 3) while resolutions of 22.62 lp/mm (group 4, element 4) and 12.7 lp/mm (group 3 element 5) were rendered for the 525 and 800 nm bands, respectively. The inferior resolution at 800 nm is attributed to cross-talk between the individual fibers of the optic image guide at this wavelength range. Fig. 2(e) shows the cross-section of the OA image of the USAF target. A line profile is also displayed, indicating an approximate resolution of 5.66 lp/mm (group 2, element 4) in the x and y directions. This corresponds to spatial resolution of 177 μ m, in good agreement with the ~5MHz bandwidth of the transducer elements.

Fig. 4 shows the sensitivity comparison results with different fluorescent dyes in phantom experiments. Both epifluorescence (Fig. 4(a)) and OA (Fig. 4(b)) images of the tubing embedded in the tissue-mimicking medium are shown for concentrations of $10 \mu g/ml$ and $50 \mu g/ml$ of ICG. While clear degradation of spatial resolution with depth is observed in the fluorescence mode, no such degradation can be recognized in the cross-sectional OA images. To quantitatively evaluate the sensitivity in detecting deeply embedded targets, image contrast for both fluorescence and OA images was calculated via [15]

$$C = (I_{sig} - I_{bg}) / (I_{sig} + I_{bg}),$$
(1)

where I_{sig} and I_{bg} are the mean pixel values of selected ROIs within the target and in the background, as indicated by the blue boxes in Figs. 4(a) and 4(b). The image contrast values as a function of target concentration and depth are shown in Fig. 4(c), in good accordance with the qualitative perception of the acquired images. This is also verified by the fullwidth-at-half-maximum (FWHM) size of the tubing in the epifluorescence and cross-section OA images, plotted in Fig. 4(d). When placed at the surface of tissue-mimicking medium (i.e. 0 mm depth), the calculated FWHM tubing diameter was 0.91 mm for fluorescence and 0.96 mm for OA. However, as the target depth increases, the tubing size broadens significantly in the fluorescence images while remaining nearly constant in the OA images. In fact, the location and shape of the tubing becomes unrecognizable in the fluorescence mode when embedded at depths beyond 2 mm in the tissue-mimicking medium. It is noted that OA signal couldn't be detected for ICG with concentration of 2 µg/ml beyond 6 mm target depth. Figs. 4(e) and 4(f) show the results for the tubing filled with AF700. The high QY of AF700 at 680 nm excitation wavelength caused fluorescence signal saturation for a concentration of 50 µg/ml at depths 0 and 2 mm and for a concentration of 20 µg/ml at a depth of 0 mm. On the other hand, the SNR of optoacoustics was very low for a concentration of 5 µg/ml at all depths and hence it was not possible to estimate the contrast and resolution of the images. The low SNR of fluorescence and OA images at certain depths also prevented the calculation of the FWHM. Figs. 4(g) and 4(h) show the corresponding results for the tubing filled with AF750. The smaller QY and larger molar extinction coefficient of AF750 with respect to AF700 results in the OA image contrast becoming superior to that of fluorescence even for relatively shallow depths. On the other hand, light scattering is reduced for longer excitation and emission wavelengths. Hence, the FWHM for the tubing filled with AF750 could still be measured in the fluorescence images at target depth of 8 mm. Figs. 4(i) and 4(j) show the results for the tubing filled with IRDye 800CW. It is shown that the performance of IRDye 800CW in terms of image contrast and resolution as a function of depth is similar to that of AF750. This is expected since both dyes have similar extinction coefficient and the excitation wavelength was the same. Note that the QY of IRDye 800CW is not available from the dye manufacturer, but it is arguably similar to that of AF750 which is corroborated in [16].

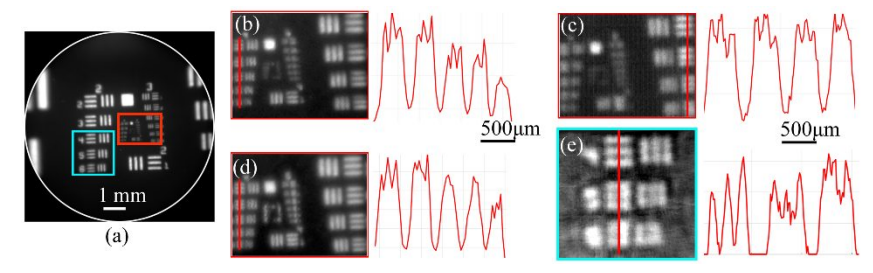


Figure 3. Spatial resolution characterization of the hybrid system. (a) Image of the entire USAF 1951 target acquired with the 525 nm band-pass filter. The white circle shows the effective FOV of the fiberscope. (b) - (d) show the zoomed-in images acquired for 525 nm, 800 nm and white light illumination and the corresponding 1D profiles along the red lines. The imaged area is indicated by red box in (a). (e) Optoacoustic image acquired from the USAF 1951 target. Single cross-section corresponding to the area indicated by a blue box in (a) is shown.

Fig. 5 shows the time-lapse fluorescence and 3D OA data acquired from the mouse brain after injection of ICG contrast agent. While superficial cortical microvasculature were clearly observed on the left (i.e., bottom) hemisphere in fluorescence image where the scalp was removed, the intact scalp over the right (i.e., top) hemisphere caused significant blurring of the underlying vasculature (Fig. 5(a)). As expected, no deterioration of image quality due to skin or skull was observed in the OA images (Figs. 5(b) and 5(c)). Three voxels with the same x and y coordinates yet different z coordinates were selected as shown in the last column in Figs 5(a)-(c) to plot the signal level versus the recording time. The signal plot of both fluorescence and OA is shown in Fig. 5(d), which displays that the average fluorescent signal level remained at its highest level at 30s (i.e., 20 s post injection) while the OA signal decreased rapidly after reaching its peak around the 17.5 s (i.e., 7.5 s post injection) time point. This can be attributed to the lack of depth resolving capability of fluorescence with its surface-weighted signal averaged across different depths.

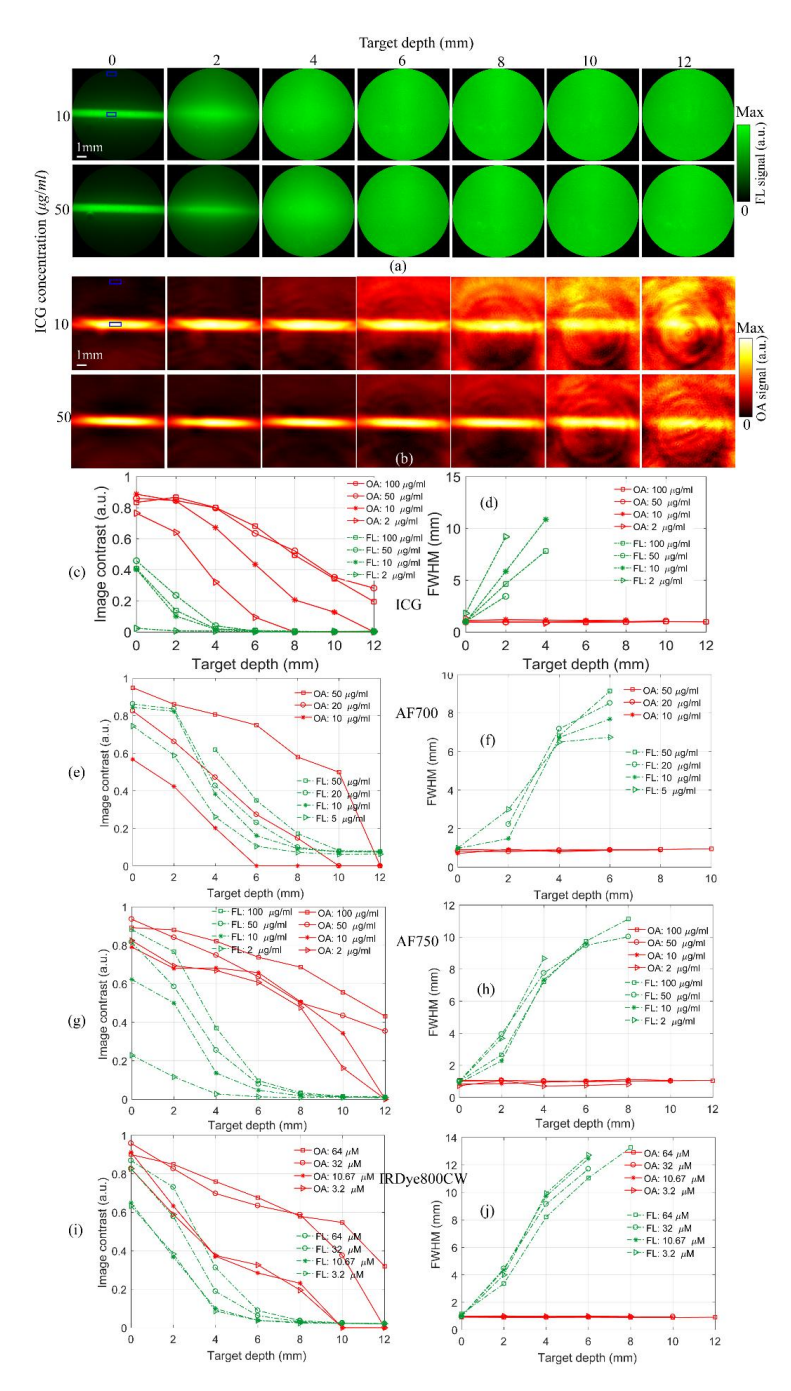


Figure 4. Experimental results of the tubing filled with ICG, Alexa Fluor 700, Alexa Fluor 750 and IRDye 800CW. (a) Fluorescence images captured at different target depths with ICG concentration of $10~\mu g/ml$ and $50~\mu g/ml$. Note that each image is normalized to itself to show details. (b) Corresponding optoacoustic single slice images. Both fluorescence and optoacoustic images were averaged over 1~s. (c) Plot of image contrast which was calculated based on the ROIs shown in (a) and (b). (d) Tubing diameter extracted from images as shown in (a) and (b) with full width at half maximum (FWHM) method. (e) and (f) Image contrast and FWHM measured from Alexa Fluor 700. (g) and (h) Image contrast and FWHM measured from Alexa Fluor 750. (i) and (j) Image contrast and FWHM measured from IRDye 800CW. Note that for those images where FWHM diameter couldn't be calculated due to low signal-to-noise ratio, FWHM values are left empty in the FWHM plot.

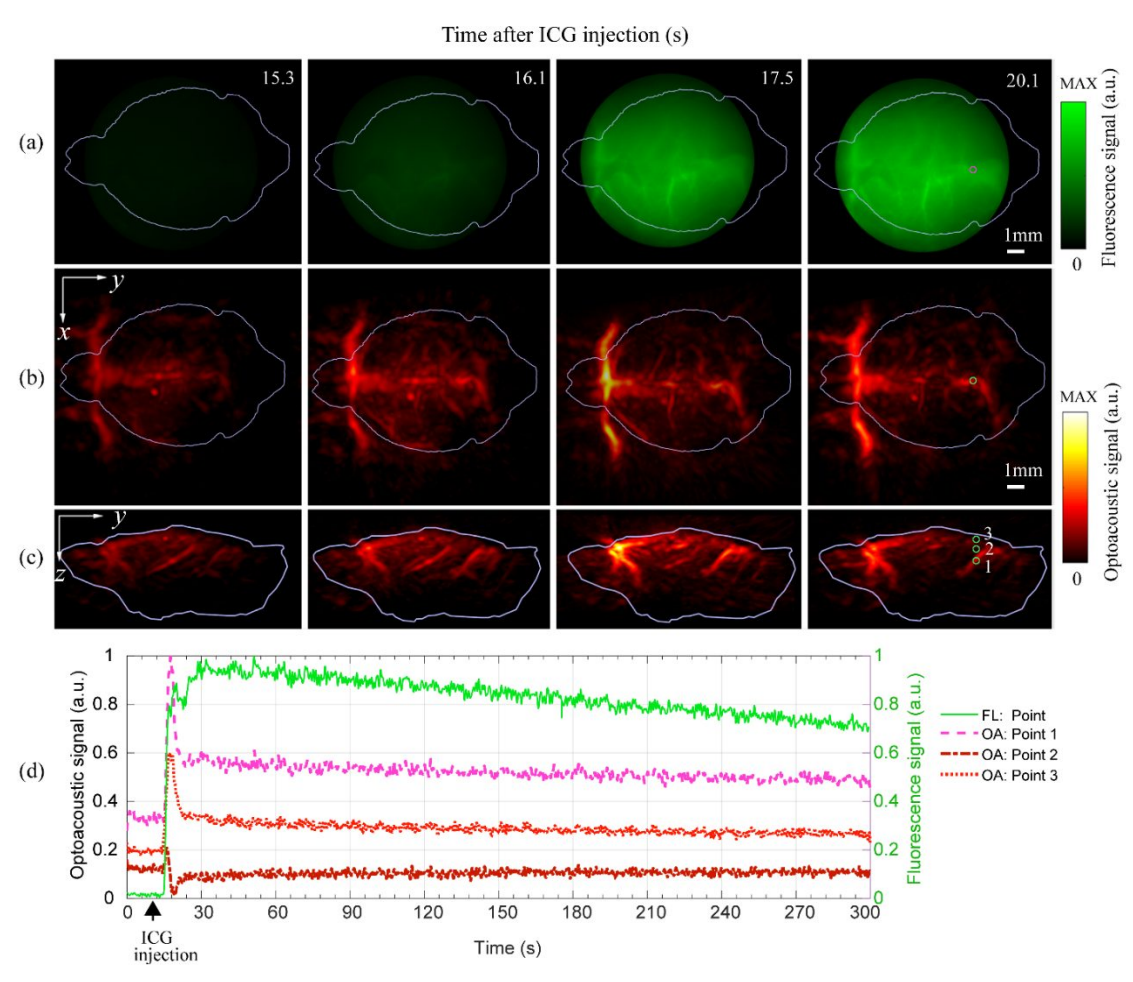


Figure 5. Non-invasive time lapse imaging of the mouse brain *in vivo* following ICG injection at t = 10. (a) Series of the epifluorescence images. (b) and (c) The corresponding volumetric optoacoustic images; maximal intensity projections along the depth (z) and lateral (x) axes are shown respectively. (d) Signal plot of epifluorescence and OA versus recording time calculated from points 1-3. Note that points 1-3 have the same x and y coordinates as displayed in (a) and (b) but different z coordinates as displayed in (c). Both fluorescence and OA signals are normalized to its respective maxima.

4. Conclusions

Our proposed solution is the first to offer hybrid fully registered fluorescence-optoacoustic imaging of living tissues across large fields of view and real-time performance both in 2D and 3D, making it especially useful for accurate monitoring of fluorescence-based signal dynamics in highly scattering samples. In addition, concurrent real-time validation with a well-established method is crucial for establishing accuracy and reproducibility of the OA imaging results. This is of particular importance for visualization of rapid *in vivo* dynamics that cannot be reliably validated on *ex vivo* specimen. On the other hand, the higher resolution of optoacoustics in deep regions enables better localization of

fluorescence agents. The proposed synergistic combination and cross-validation of fluorescence and optoacoustic imaging can therefore benefit numerous studies looking at multi-scale *in vivo* dynamics, such as functional neuroimaging, visualization of organ perfusion and contrast agent uptake, cell tracking, pharmacokinetic and biodistribution analysis.

ACKNOWLEDGEMENT

The authors would like to acknowledge grant support from European Research Council (ERC-2015-CoG-682379), US National Institute of Health (R21-EY026382), Human Frontier Science Program (RGY0070/2016) and Deutsche Forschungsgemeinschaft (RA1848/5-1)

REFERENCES

- [1] Razansky, D., Distel, M., Vinegoni, C., Ma, R. and Perrimon, N. "Multispectral opto-acoustic tomography of deep-seated fluorescent proteins in vivo," Nat Photon. 3,412-417 (2009).
- [2] Dean-Ben, X. L., Gottschalk, S., Mc, L. B., Shoham, S. and Razansky, D. "Advanced optoacoustic methods for multiscale imaging of in vivo dynamics," CHEMICAL SOCIETY REVIEWS. 46(8),2158-2198 (2017).
- [3] Wang, B., Zhao, Q., Barkey, N. M., Morse, D. L. and Jiang, H. "Photoacoustic tomography and fluorescence molecular tomography: A comparative study based on indocyanine green," MEDICAL PHYSICS. 39(5),2512-2517 (2012).
- [4] Razansky, D. and Ntziachristos, V. "Hybrid photoacoustic fluorescence molecular tomography using finite element based inversion," MEDICAL PHYSICS. 34(11),4293-4301 (2007).
- [5] Kim, C., Song, K. H., Gao, F. and Wang, L. V. "Sentinel lymph nodes and lymphatic vessels: noninvasive dual-modality in vivo mapping by using indocyanine green in rats--volumetric spectroscopic photoacoustic imaging and planar fluorescence imaging," RADIOLOGY. 255(2),442-450 (2010).
- [6] Kosik, I. and Carson, J. J. L. "Combined 3D photoacoustic and 2D fluorescence imaging of indocyanine green contrast agent flow," Proc. SPIE. 8581858143 (2013).
- [7] Rao, B., Soto, F., Kerschensteiner, D. and Wang, L. V. "Integrated photoacoustic, confocal, and two-photon microscope," JOURNAL OF BIOMEDICAL OPTICS. 19(3),36002 (2014).
- [8] Wang, Y., Maslov, K., Kim, C., Hu, S. and Wang, L. V. "Integrated photoacoustic and fluorescence confocal microscopy," IEEE TRANSACTIONS ON BIOMEDICAL ENGINEERING. 57(10),2576-2578 (2010).
- [9] Deán-Ben, X. L. and Razansky, D. "On the link between the speckle free nature of optoacoustics and visibility of structures in limited-view tomography," Photoacoustics. 4(4),133-140 (2016).
- [10] Chen, Z., Deán-Ben, X. L., Gottschalk, S. and Razansky, D. "Hybrid system for in vivo epifluorescence and 4D optoacoustic imaging," OPTICS LETTERS. 42(22),4577-4580 (2017).
- [11] Thermo Fisher Scientific, The Alexa Fluor Dye Series Note 1.1.
- https://www.thermofisher.com/de/de/home/references/molecular-probes-the-handbook/technical-notes-and-product-highlights/the-alexa-fluor-dye-series.html
- [12] Goutayer, M., Garcia, F. N. Y. and Texier-Nogues, I., Fluorescent emulsion of indocyanine green: Google Patents, 2016.
- [13] IRDye® 800CW Maleimide. https://www.licor.com/bio/products/reagents/irdye/800cw/maleimide.html
- [14] Steven, L. J. "Optical properties of biological tissues: a review," Physics in Medicine & Biology. 58(11),R37 (2013).
- [15] Michelson, A. A., Studies in optics, The University of Chicago Press: Chicago, Ill. (1927).
- [16] Qin, Z., Hall, D. J., Liss, M. A., Hoh, C. K., Kane, C. J., Wallace, A. M. and Vera, D. R. "Optimization via specific fluorescence brightness of a receptor-targeted probe for optical imaging and positron emission tomography of sentinel lymph nodes," JOURNAL OF BIOMEDICAL OPTICS. 18(10),101315 (2013).